JOURNAL OF SPACECRAFT AND ROCKETS
Vol. 29, No. 2, March-April 1992

Thermal Protection Analysis of Mars-Earth Return Vehicles

William D. Henline*
NASA Ames Research Center, Moffett Field, California 94035

An analysis is performed to determine the aerothermodynamic heating and thermal protection materials requirements of a typical "fast" manned Mars mission. Entry conditions represent those consistent with an early manned mission having a total trip time of approximately 14–16 months. A coupled flowfield-radiation stagnation region heat transfer viscous shock layer (VSL) calculation was performed to ascertain the various shock layer heating mechanisms and the resultant surface heat fluxes for a generic shaped Mars/Earth return capsule. Computations were performed using the VSL computer code, RASLE. The ablation and thermal response of four different candidate ablating heat shield materials was determined using results from the RASLE code in conjunction with the detailed (one-dimensional) charring ablator-thermal response code CMA. Based on these results, the Earth return capsule thermal protection system (TPS) mass fraction was estimated for each material. A general conclusion is that attractive TPS mass fractions of 10–15% are possible with these candidate systems but that a vehicle and mission dependent choice must be made between heat shield total surface recession and initial TPS mass fraction.

Nomenclature

B'_c = dimensionless ablative mass loss rate
B'_g = dimensionless pyrolysis gas rate
C_H = surface, blowing value of film heat transfer coefficient, kg/m^2-s
C_H^0 = nonblowing surface, film heat transfer coefficient, kg/m^2-s
H_r = recovery enthalpy behind blow shock, J/kg
L/D = vehicle lift-to-drag ratio
$\dot{m}_c$ = ablation mass loss rate, kg/m^2-s
P_e^0 = stagnation pressure, kPa
Q_c = net surface convective heat flux, MW/m^2
Q_R^E = surface emitted radiative heat flux, MW/m^2
Q_R^I = net incident radiative heat flux, MW/m^2
Q_R^{Ref} = surface reflected radiative heat flux, MW/m^2
R_N = entry capsule nose radius at stagnation point, m
T = local temperature, K
t = trajectory time, s
U_e = tangential velocity at boundary-layer edge, m/s (for use in boundary-layer-based heat transfer correlations)
U_S = tangential velocity adjacent to shock, m/s
V_∞ = freestream velocity
β = vehicle ballistic coefficient, kg/m^2
Δ = shock standoff distance, m
$\mu_\nu^{(i)}$ = spectral absorption coefficient for radiative process (i)
ν = frequency or kinematic viscosity
ρ = density, kg/m^3

Subscript

∞ = freestream condition

Presented as Paper 91-0697 at the AIAA 29th Aerospace Sciences Meeting, Reno, NV, Jan. 7–10, 1991; received April 26, 1991; revision received Sept. 30, 1991; accepted for publication Sept. 30, 1991.

*Research Scientist, Thermal Protection Materials Branch.

Introduction

FUTURE manned exploration missions to Mars are currently undergoing serious consideration by NASA and other U.S. scientific establishments. Among the current heavily debated options for mission vehicle modes is the choice between use of propulsive vs aerodynamic deceleration. There are, within each of these options, many different tradeoffs needed to obtain a workable transportation system. One mission element is, however, becoming increasingly clear. At least for the early manned Mars missions, it appears that the final Earth return will probably require a vehicle that is large enough to carry the five to six crew members and a small amount of Mars surface material. This capsule will execute Earth orbital injection using an aerobraking maneuver or, optionally, perform a direct entry to the surface in much the same fashion as the Apollo lunar return. It is desired to establish the flight trajectory and aerothermodynamic heating environment for such a manned vehicle and to determine the state of the art and future thermal protection system (TPS) materials necessary and available to protect the vehicle in that environment. Computations made here are intended to be accurate enough to assist in definition of required vehicle generic shapes and to provide heat shield mass comparisons for different TPS materials. The results are by no means meant to represent the vehicle heat shield final design.

Tauber et al.[1] have performed an extensive investigation of both the Mars entry and Mars/Earth return trajectory parameters and have analyzed the effects these have on vehicle shape, L/D, and ballistic coefficient β required to perform these entry flights and still satisfy the imposed crew g-load limits and the onboard guidance, navigation, and control constraints. Some entry vehicle heating analysis was also performed, but for a cold (nonablating) wall. These results will be the starting point for the analysis in the present study. To further establish the entry heating conditions, a stagnation region radiation transport-coupled viscous shock layer (VSL) surface heating analysis was performed for the candidate entry vehicle. As will become obvious from the analysis that follows, the heat shield TPS required for Mars/Earth return must be an ablator at least in the vicinity of the stagnation point. Since ablating systems operate partially by convective blocking through shock layer mass injection, both radiative and convective surface heating will intimately depend on the actual nature of the injected material. Radiative VSL heating calculations were therefore made for the candidate material systems of interest. These include both carbonaceous and silica-based materials.

Transient thermal response and surface recession studies were made for four candidate ablator TPS materials, using the results from the VSL heating calculations and the trajectory studies of Ref. 1. Those materials are carbon phenolic, carbon-carbon, Apollo (Avcoat) ablator, and low-density silica fiber based insulative/ablator (NASA LI-2200 Shuttle tile) materials. These analyses were made using the well-known ACE[2] thermochemical equilibrium and CMA[3] transient response computer codes. Included in these computations were estimates of insulation material thicknesses required to maintain allowable structural temperatures throughout a prolonged heat soak period. Comparison estimates of TPS weight loading were then made to establish the relative merits of each material for application to the return capsule. In the sections that follow, a detailed description of each of these considerations is presented.

Mars/Earth Return Entry Trajectories and Required Vehicle Configurations

As discussed by Tauber et al.,[1] under the premise that the initial manned Mars missions will return only the crew and small amounts of surface material to Earth, the return vehicle must be selected and designed to conform to a mission scenario that favors maximum performance and safety of the crew. Among such considerations are certainly mission duration and g-loads experienced by the crew during various phases of the flight. It appears that there is some consensus toward relatively fast missions based on chemical propulsion and vehicle aerobraking both at Mars and Earth.[4] Fast missions will result in higher aerobrake entry velocities at both planets. The TPS weight fraction can be minimized by keeping Earth entry velocities at or below 12.5 km/s as a nominal operation value. However, it is also apparent that flight contingencies could require designing the entry capsule to safely aerobrake at velocities as high as 14 km/s. This will be the design case in the present study.

Again referring to Ref. 1, that study investigated a range of vehicle L/D and ballistic coefficients β and the resultant effect on trajectory parameters and surface heating. One important constraint to consider is the upper limit on g-load which the crew can tolerate after a long space journey at zero gravity. NASA has tentatively set such a limit at 5 g. With this constraint, for example, an Apollo shaped vehicle with an L/D of 0.3 (at an angle of attack of 25 deg) will have a prohibitively narrow entry corridor of 0.3 g at the 5 g limit for a 14 km/s entry. It is doubtful that current guidance, navigation, and control can achieve this kind of performance margin. Vehicle performance at maximum g-load does not appear to be a sensitive function of the ballistic coefficient. However, surface heating has a direct dependence on β. In Ref. 1, by examining a range of L/D of 0.2 to 0.5 and β of 300 to 500 kg/m^2, it was determined that at 14 km/s entry velocity, a generic raked-cone geometry flying at 0-deg angle of attack and having an L/D of 0.5 and β of 300 kg/m^2 will provide an entry guidance corridor margin of approximately 1 deg for a g-load limit of 5 g. Preliminary surface heating estimates were found to range from 9.0 to 13.3 MW/m^2 based on cold-wall convective and radiative heating analyses, but still requiring ablative TPS materials. Figure 1 (Ref. 1) shows a sketch of the generic vehicle geometry in question. The configuration is based on a blunted, slightly elliptical cross-section raked cone with average nose radius of 1 m and a base diameter of 5.2 m. A direct entry trajectory altitude vs time plot for this entry capsule, also from Ref. 1, is shown in Fig. 2. Trajectories are illustrated for both the undershoot and overshoot flight paths.

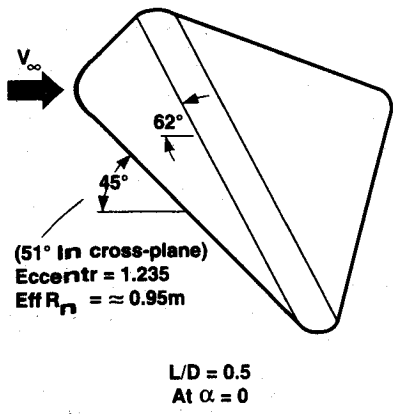

Fig. 1 Entry configuration studied.

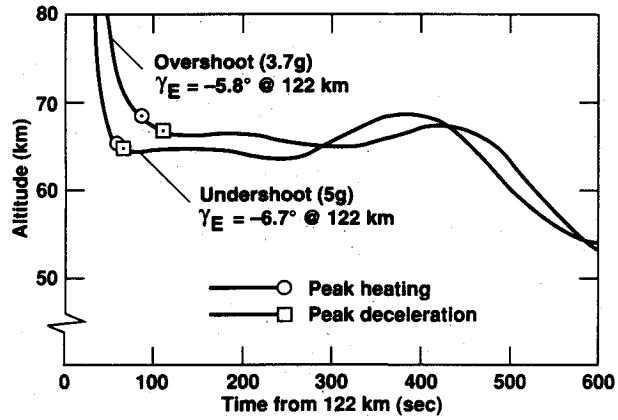

Fig. 2 Earth direct entry trajectories,[1] V_e = 14 km/s, L/D = 0.5, β = 300 kg/m^2.

A primary goal of the current study is to provide an aerothermodynamic heating analysis for the Mars/Earth return capsule (cf. Fig. 1) discussed above, for different candidate TPS materials. The heating results will then be used to define the thermal and recessional response of these materials. From this it is then possible to more clearly define the range of TPS material requirements and material types needed in any future vehicle/mission optimization trade study.

Analysis of Aerothermodynamic Heating Environment

As shown above, an entry vehicle of the required type arriving at Earth from Mars at 14 km/s will encounter very high peak stagnation point heating rates ($\approx$ 10.0 MW/m^2). To mitigate this would require a TPS material capable of withstanding operating temperatures in excess of 3600 K if the only heat rejection mechanism were radiative cooling. There are currently no such materials. Additional dissipation mechanisms must therefore be included, and one efficient means is through the use of ablative materials for the heat shield. Ablators can accept large amounts of surface energy input by endothermic, pyrolytic breakdown of the resident material. In addition, at the high operating temperatures of these TPS, the surface can undergo sublimation or vaporization with the associated vapor carrying a significant latent heat of vaporization away from the surface. Finally, the ablation mechanism introduces a convective mass flux into the shock layer to actively block the incoming convective and radiative energy flux.

At the heat flux levels encountered in ablating systems, shock layer radiative heating processes become significant and eventually dominate as the entry speed exceeds hyperbolic values of 11 km/s for Earth. Any entry vehicle heating analysis that is to be definitive will have to therefore account for the combined dissipation mechanisms of flowfield shock-generated radiation, mass addition at the surface, convection/conduction, and surface radiation absorption and emission in the presence of a reacting real gas flowfield. Computer simulation codes that do this are very few in number; only two have been

successfully applied to the present type of problem. These include the HYVIS code from NASA Langley Research Center[5] and the RASLE code used at NASA Ames Research Center.[6] Both codes were developed to simulate the radiation-dominated ablating flowfields encountered in Jovian entry. The NASA Galileo probe to Jupiter is protected by a carbon-phenolic forebody heat shield designed with the aid of these two computer codes.

In a manner similar to the Galileo probe, the RASLE VSL computer code has been used in this study to more carefully define the heating environment of the Mars/Earth return capsule. Using results from RASLE, the present study compares the effects of the heating environment on various TPS materials. Although four separate materials have been studied, all fall into two generic systems relative to RASLE. These can be approximated by either a hydrocarbon (carbonaceous) or silica (SiO_2) ablating-radiating shock layer problem. Both steady-state ablation and nonablating (reference) calculations were done for each of these systems using the RASLE code. Each requires a comprehensive, thermodynamic and transport property input data set. Reference nonablating calculations are necessary to establish blowing factor corrections for later thermal response analysis using CMA. The details of this calculation and the results are presented in sections that follow. Before this, however, it will be informative to briefly discuss the capabilities and characteristics of the RASLE code and the associated radiation transport model.

Radiatively Coupled Viscous Shock Layer Code RASLE

This program is designed to solve the coupled problem of a nongray radiating gas and the hypersonic, thin-layer viscous shock, external body flow. The flowfield is coupled with a general radiation ablating surface mass and energy balance boundary condition. Flight conditions during peak heating are primarily in the continuum flow region, and pressures (and total enthalpies) are assumed to be high enough that the shock layer is in thermochemical equilibrium. There have been recent studies by Gupta et al.[7] and Mitcheltree and Gnoffo[8] both confirming and invalidating this assumption, respectively. In all likelihood, further study will be needed to reach a final conclusion. Both laminar and turbulent flow conditions can be modeled. Viscous shock flowfield governing equations are written in the thin viscous shock approximation for a body-fixed coordinate system. An equilibrium real gas thermochemical model is assumed here and employs a simplified binary diffusion model due to Lees.[9] As mentioned earlier, these equations must be solved subject to the appropriate boundary conditions at the bow shock and at the body surface. In this case boundary conditions at the shock are the usual hypersonic, equilibrium Rankine-Hugoniot adiabatic shock relations. At the ablating surface, boundary conditions may be specified by fixing temperature and species composition or determined through the simultaneous constraints of mass, momentum and energy conservation at surface conditions obtained during the course of solution.

Solution of these governing equations is by the finite difference method. As described in Ref. 6, the shock layer is divided into two zones between the shock and body surface. Forward difference relations are used in the zone adjacent to the body, whereas the outer region near the shock employs backward difference relations. The two regions are joined by matching adjacent interior nodes with higher order splines. The solution of the overall elliptic type Cauchy problem is approximated through the use of a hypersonic bow shock correlation developed by Falanga and Olstad.[10] Together with the equilibrium normal shock standoff (determined by the code) a stagnation streamline and downstream solution, in principle, can be obtained. This solution procedure is globally iterated from the shock correlation to ultimately yield the desired body shape. It is, in a sense, a classical blunt body inverse solution procedure. A primary mathematical difficulty in solving this equation set is the evaluation and coupling of the local radiative flux with the total energy equation. To do this the RASLE code was developed to include a very extensive nongrey radiative transfer model. An abbreviated discussion of this model is given here.

RASLE Detailed Radiation Model

The radiative transport model included in RASLE was developed by Nicolet[11] and Wilson and Nicolet.[12] It is extensive and is designed to be essentially complete with perhaps two exceptions. When considering hypersonic flows over planetary entry vehicles, it is assumed that flight regimes of interest (specifically where high heating rates occur) will be in the near transitional and continuum flow region. If this is not true, two radiation limiting processes will occur; namely, collision limiting and general nonequilibrium radiation. The RASLE radiation model is not capable of representing these latter two low-density (high-altitude) related phenomena. In the future, these limitations can perhaps be removed without giving up generality of the radiation shock layer physics or ease of flowfield/radiation computations. The present model is a detailed spectral representation of the dominant radiative processes in a general multicomponent radiating gas. It is assumed that the gas is locally in radiative equilibrium and is allowed to both absorb and emit, but scattering is neglected. Radiation at the body surface can be emitted spectrally and reflected diffusely but cannot be transmitted in depth. To approximately account for the nonzero view factor with respect to more intense radiation from the stagnation region, the local radiative flux can have an angular dependence. Except for this feature, the radiation model is locally one dimensional in the sense of the tangent slab approximation.

Final integration of the energy equation, including the radiative flux integral, requires knowledge of the spectral gas absorption coefficient μ_ν as a function of position in the shock layer. Herein lies most of the radiation physics in that the absorption coefficient of a radiating plasma is dependent on all of the various radiating processes. In particular, μ_ν can be expressed as the linear combinant sum,

$$\mu_\nu = \sum_{i=1}^{N_c} \mu_i^C(\nu) + \sum_{k=1}^{N_L} \mu_k^L \qquad (1)$$

The first summation represents the contribution from continuum radiation and is taken over all N_c continuum transitions, and the second term is the contribution from line radiation summed over all N_L line transitions. Individual terms in the μ_ν summation that are significant for the high enthalpy re-entry flow are outlined briefly in the following section. The radiation model that these specific functional forms represent is due to Nicolet,[11] and reference should be made to that work for an in-depth discussion of the theory.

Continuum Contributions

Contributions to μ_ν^C are included from both atomic continua and molecular processes. Among the atomic continua, contributions are included to account for free-free and bound-free events. The bound-free events include photoionization and photodetachment. For purely hydrogenic systems, cross sections for the free-free and bound-free transitions are well understood and can be written in direct analytical form. These expressions can be found in Ref. 11. For the more practical, heavy ion systems, the most reliable results have been obtained from the so-called "quantum" defect method. In RASLE this method is implemented as follows. In the low frequency regime, Biberman and Norman's[13] approximation is applied to the photoionization and free-free transitions. The remaining portion of the spectrum must be represented explicitly through knowledge of actual event cross sections. These are tabulated for many atomic and ionic systems in the extensive work by Peach.[14] A synopsis of the necessary cross sections used in this work can be obtained from Ref. 15. For air systems, the O_2 Schumann-Runge photodissociation contin-

uum is the most important contributor to this process. Cross-section information for this contribution is available from Evans and Schexnayder.[16] Additional contributions due to photodetachment for O^-, C^-, and H^- have been included from various investigators.[17-19]

Molecular continuum processes include the pseudocontinua of molecular rotational and vibrational lines and are modeled by the bandless approximation model. Individual data and correlations for selected species have been obtained from various resources (cf. Ref. 6) and are included in the RASLE code. Specifically, correlations are available for N_2^+, NO, O_2, N_2, CO, CN, C3, and SiO molecular systems.

Atomic and Ionic Line Transitions

Radiation due to spectral line transitions is evaluated in a statistical manner similar to the atomic continua. In addition, however, a configurational parameter is required to represent the functional form (shape) of the individual lines. The RASLE radiation model accounts for Stark, resonance, and Doppler broadening effects. The code allows for up to 20 line groupings. Within each frequency group the total line group contribution is obtained by summing the individual contributions within that group. Specific details of the actual implementation of this group model are given in Refs. 11 and 12. Oscillator strengths for individual lines due to the various atom and ion systems of interest were obtained from Moore.[20]

Stagnation Streamline RASLE Solutions for Manned Mars Return

Using the detailed radiation model and approximate VSL capabilities of RASLE, it was desired that definitive, combined convective-radiative heating computations be made for the most probable trajectory and vehicle configuration for the manned Mars/Earth return mission. Since the ultimate goal is to compare different TPS materials for specific vehicle configurations, calculations were done only for the stagnation streamline of the generic vehicle of Fig. 1. For sphere-cone geometries, full forebody RASLE or HYVIS solutions are very difficult to obtain. This is due to the effects of the discontinuity occurring in the second derivative of the body geometry surface function at the sphere-cone junction. This problem can be a serious one for cone half-angles greater than 50 deg. In that case, stagnation point heating is significantly influenced by the extreme bluntness of the geometry. To accurately determine stagnation heating from a VSL code like RASLE, an effective nose radius (larger than actual) would have to be used. The geometry used here is a 45-deg sphere cone and should not require the use of the effective nose radius artifice, particularly in light of the comparative nature of this analysis.

As mentioned earlier, although there are four actual TPS materials being compared here, only two generic material systems were calculated in detail using RASLE. These are the carbon-hydrogen-air and silicon-air systems. To perform such computations, it is required that all of the system radiation property data, component thermodynamic and transport coefficients, as well as material surface radiation boundary conditions be supplied. Of course, the flight condition freestream conditions are needed, and the manned Mars return, 14 km/s, undershoot trajectory maximum heating point conditions used here are shown in Table 1.

Heat capacity data has been obtained from the JANNAF[21] thermochemical data base, whereas transport coefficients are calculated from collision integrals using the methods outlined by Yos.[22] Obtaining radiation property and cross-section data is a difficult task, and for this reason, the values obtained for this study have been tabularized by the author.[15] In this tabulation, the atomic and ionic line transition properties and oscillator strengths (f numbers) for the carbon-hydrogen-air and silicon-air systems are given. Also listed are the frequency line centers for all of the appropriate line transitions included in the calculation. However, not all of the associated energy levels are actually used. A maximum of eight lumped levels are allowed. In addition to line centers and f numbers, Ref. 15 also lists species line parameters needed to implement the RASLE line-averaging model, as well as species explicit photoionization cross-section information obtained from Wilson and Nicolet[12] and Peach.[14]

Surface, radiative boundary conditions can have a significant effect on the final surface heating values. It was assumed that the hydrocarbon system (char) had a gray surface with the relatively high, constant emissivity of $\epsilon = 0.9$. However, it is known that SiO_2 surfaces can have a spectrally dependent emissivity. Recent experimental ablation studies of LI-2200 RSI material in the NASA Ames Research Center 60-MW IHF arc jet,[23] however, indicate that the high temperature, ablating surface can be approximated as having a total hemispherical emittance of $\epsilon = 0.4$. Since this material is representative of the SiO_2 air system, this constant emissivity was assumed for the present study.

Four specific calculations were carried out with the RASLE code for the 14 km/s maximum heating trajectory point. For both the carbon-hydrogen-air and silica-air cases a nonablating calculation was performed as a reference to complimentary steady-state ablation solutions. These nonablating solutions were obtained to ascertain material specific shock layer empirical blowing parameters for use in subsequent ablative material transient thermal response calculations. It is important that these nonblowing VSL solutions represent a physical shock layer flow that is in some way equivalent to the associated ablation case. However, the two situations cannot be mathematically equivalent. The choice was made here to have the nonablating case be thermochemically equivalent at the material surface by imposing the same surface temperature (as a boundary condition) that was obtained in the corresponding ablating calculation. By making this imposition, the nonablating cases will not be equivalent to the ablating solutions with respect to the resultant surface energy balances. The fixed wall temperature boundary conditions (nonblowing) are nonadiabatic at the wall, with some material in-depth conduction of energy implied. The ablating cases impose an adiabatic (steady-state) back wall energy balance with no in-depth conduction. These inconsistencies are inherent in any uncoupled shock layer/transient thermal response calculation. They will be not be of direct consequence in the present analysis because the shock layer results and thermal response calculations are coupled only through the "blowing parameter" obtained from the previously described reference RASLE solutions.

An additional approximation is being made here in the use of the so-called "steady-state ablation" solutions obtained for the maximum heating point of the Mars return entry trajectory. This will be a good approximation in high net heat flux situations similar to the present cases. Also, the shorter the duration of the heat pulse, the better the approximation. The trajectory studied here has a heat pulse duration of the order of 2 min, and is probably long enough to allow some in-depth

Table 1 Manned Mars/Earth return flight conditions, 14 km/s, maximum heating condition undershoot trajectory

Freestream conditions
$V_\infty = 13{,}200$ m/s
$\rho_\infty = 1.7 \times 10^{-4}$ kg/m^3
Initial entry angle
$\gamma_E = -6.6$ deg
Vehicle parameters
$R_N = 1$ m
$\beta = 300$ kg/m^2
$L/D = 0.3$
Maximum acceleration
5 g

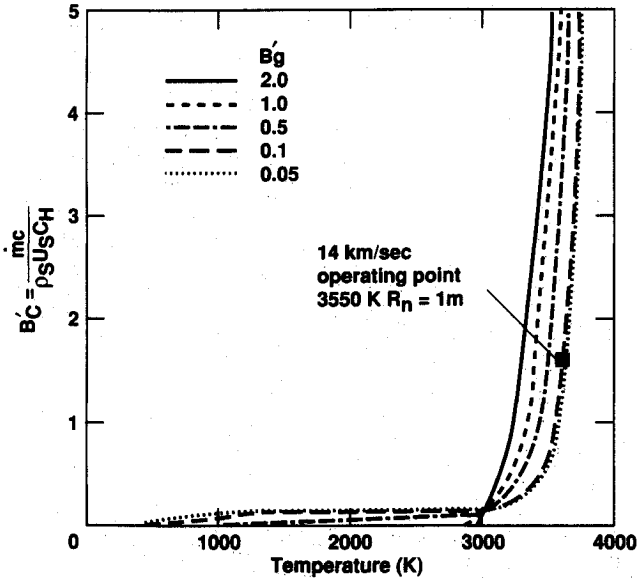

Fig. 3 B'_c curve for carbon phenolic, $P_e^0 = 0.275$ atm.

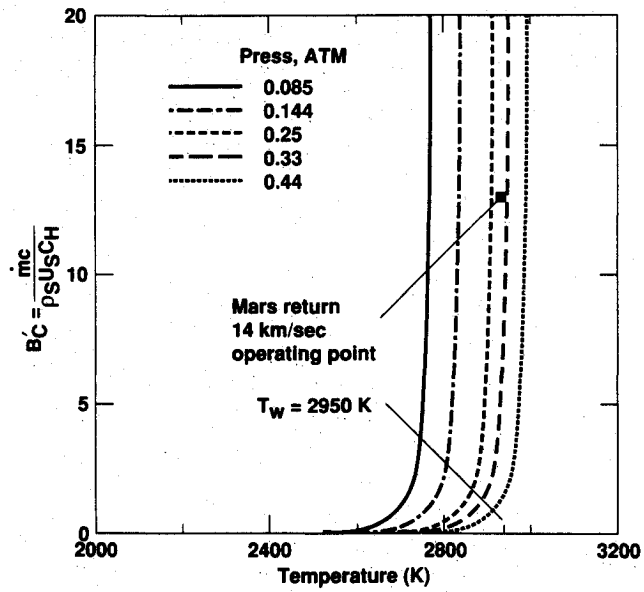

Fig. 4 B'_c curve for SiO_2 in air.

conduction for some materials. The consequences of this are discussed later.

The present analysis has included a refinement on the surface mass and energy balance boundary conditions employed for the ablating cases. Vaporizing hydrocarbon and silica systems will lose mass at rates constrained by the limits of the material vapor pressure-temperature relationships in air. Vapor pressure curves in the form of dimensionless mass loss B'_c curves obtained from ACE[2] are shown in Figs. 3 and 4 for carbon-phenolic and SiO_2 in air, respectively. For the ablating cases, RASLE was run for an assumed (trial) fixed surface temperature. The resultant ablation mass flux was then used to iterate with each B'_c curve until (at a fixed pressure) an invariant B'_c surface temperature point was obtained. As shown in Fig. 3 for carbon phenolic, the stagnation point surface operates at about 3550 K, whereas that for SiO_2 is at 2950 K. Both of these temperatures are slightly lower than the respective equilibrium vaporization temperatures of 3950 and 2975 K. Slightly higher heating rates would then drive the surface to these higher equilibrium values and no iteration would be needed for solution. Comparison of these temperatures and ablation rate results will be made with the in-depth CMA ablation-recession calculations.

The results of these simulations for the 1-m nose radius Mars return capsule (stagnation point) are presented here in tabular and graphical form. Table 2 shows a summary of the total and individual surface heat fluxes for all of the cases considered. Mass loss rates are given for the ablating cases. At first glance there appear to be some inconsistencies in these results. The nonablating cases have greatly different surface "convective" heat fluxes. The carbon-phenolic values are almost twice those for the silica system. If radiation was not a significant component of the heating mechanism, these results would indicate an improper solution. Figure 5 presents stagnation streamline temperatures for each of the four cases listed in Table 2. Temperature gradients for the nonablating case are indeed different, and the blowing cases show the surface gradient reduction attendant to mass injection. The matched surface temperature for ablating and nonablating cases is also apparent. As is proper with the Rankine-Hugoniot equilibrium shock conditions imposed here, all temperature pro-

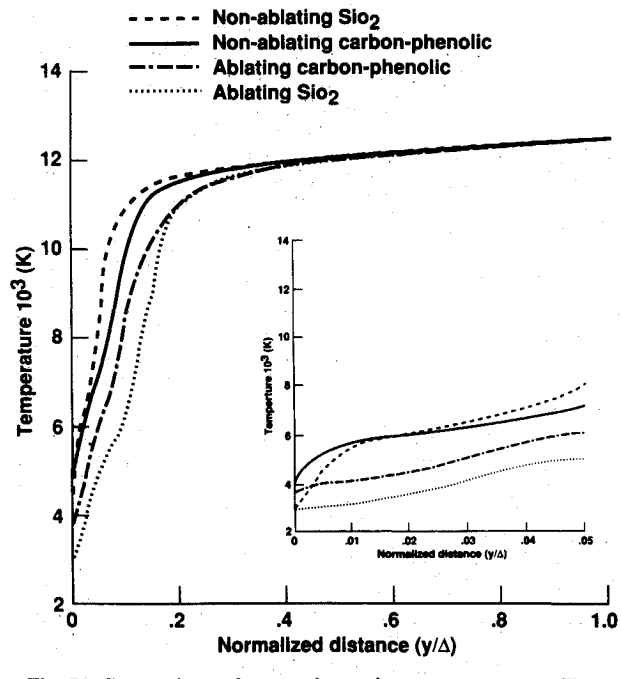

Fig. 5 Comparison of stagnation point temperature profiles.

Table 2 14 km/s Mars/Earth return RASLE simulation peak stagnation point heating-ablation results, $P_e^0 = 27.86$ kPa, $R_N = 1$ m

Q_c, MW/m²	Q'_R, MW/m²	Q_R^{Ref}, MW/m²	Q_R^E, MW/m²	$\dot{m}_c$, kg/m²-s
		Carbon phenolic		
4.48	5.15	0.515	7.63	0.0962
11.81	5.82	0.58	7.97	0.0
		SiO_2		
2.18	5.41	3.25	1.59	0.183
8.29	5.79	3.48	1.57	0.0

files converge at the shock. Figure 6 shows stagnation layer profiles for the individual diffusive (conduction plus energy transport due to mass diffusion) and radiative heat fluxes for the nonablating cases. The carbon-phenolic and silica systems are mathematically identical except at the boundaries. There are slight differences in the surface temperatures and large differences in the surface material emissivities. The higher carbon-phenolic emissivity ($\epsilon = 0.9$) results in a much higher emitted surface radiative flux than for the silica case ($\epsilon = 0.4$). The carbon-phenolic shock layer is radiatively cooled everywhere, whereas the silica case is radiatively heated near the surface. At the surface, where purely convective fluxes are zero (as opposed to conduction and diffusion), a summation of diffusive and radiative energy flux for each case agrees to within 1.5%. Attention must be paid to the proper sign convention required for radiation flux (cf. Fig. 6). The slight difference in net surface flux between carbon-phenolic and silica systems is due to the small difference in surface temperatures. Thus, it can be concluded that these two solutions are consistent and that an overall shock layer energy balance is in force. What appears to be an inconsistency is the result of

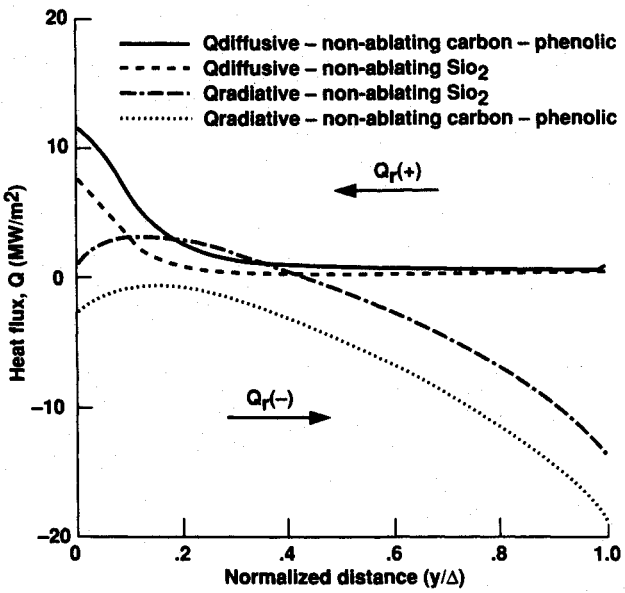

Fig. 6 Nonablating component stagnation point heat flux profiles.

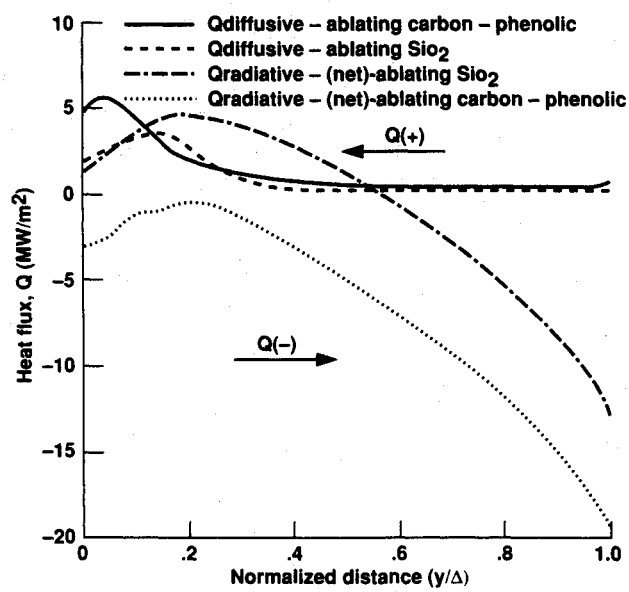

Fig. 7 Ablating component stagnation point heat flux profiles.

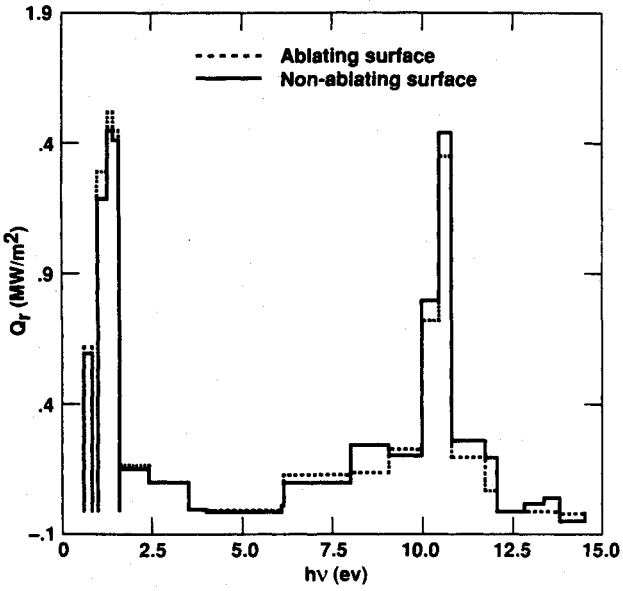

Fig. 8 Carbon-phenolic line radiative flux comparison.

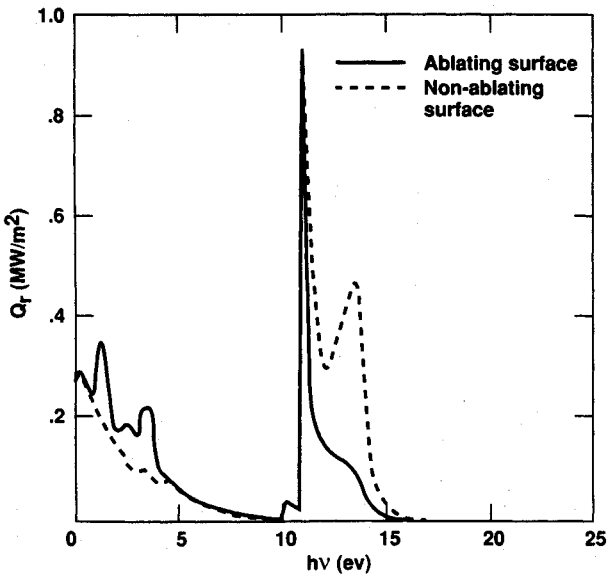

Fig. 9 Carbon-phenolic continuum radiative flux comparison.

intuitive notions derived from previous experience with uncoupled shock layer/radiation calculations and does not pertain to the tangent slab, coupled results obtained in this study. Equivalent heat flux profiles for the ablating cases are presented in Fig. 7. The diminution of diffusive surface flux is evident, whereas it is less so for radiation.

As shown in Table 2, material surface response is quite different between the two cases. Even though the silica surface reflects approximately 60% of the incident radiation, it emits only about 7–10% (in the ablating case) of the incident value. The net result of the remaining convective and radiation input results in about twice the ablation mass loss rate for silica systems over carbon-phenolic systems. This, however, results in the advantage of much higher surface convective heat flux attenuation for silica. To further decide on the relative merits of these two material types, a more detailed trajectory based CMA thermal response analysis is needed. This is discussed in the next section.

Since the calculations performed here are based on a completely coupled, spectral radiation model, it is possible to obtain values of the spectral radiative energy flux at any point in the flowfield. This is available for both the line and contin-

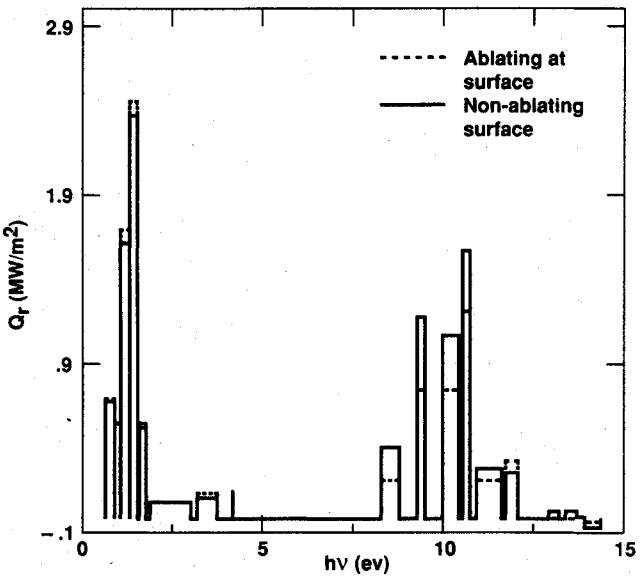

Fig. 10 SiO_2 spectral line radiative fluxes.

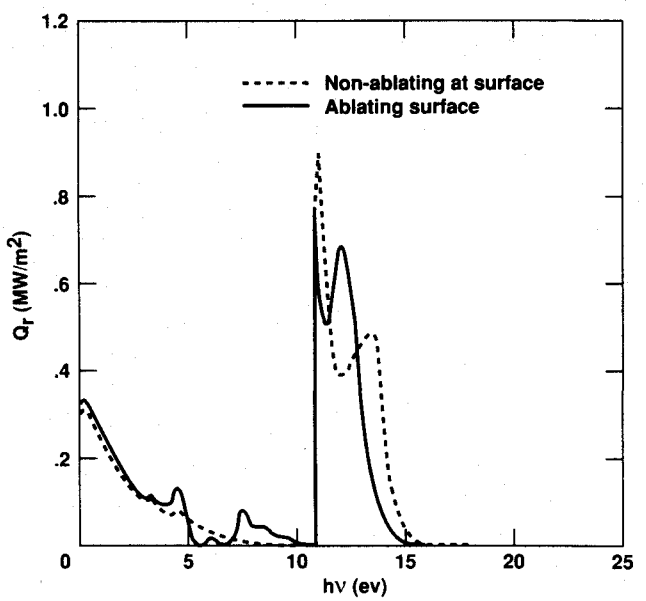

Fig. 11 SiO_2 continuum radiative flux comparison.

uum radiation components, and detailed plots of surface spectral fluxes are shown in Figs. 8–11 for both ablating and nonablating carbon-phenolic and SiO_2 systems, respectively. Generally speaking, continuum fluxes are higher in the carbon system, whereas line radiaton values are somewhat higher in the silica system. Both systems display the classical behavior with regard to flux attenuation by the relatively cold wall shear layer (boundary layer). However, as Figs. 10 and 11 show, the radiative blockage effects of the ablating SiO_2 system are minimal. Also it can be seen from Figs. 8–11 that radiative blockage is not uniform over the entire spectrum. Both the line and continuum radiation flux plots show that most of the blockage occurs in the uv region above 10 eV. Figure 12 is a spectral plot of total radiation flux for each of the calculations. The visible and ultraviolet regions provide most of the radiative heating contributions. This comparison also shows (as indicated earlier) that ablative product blockage of radiation is effective only in attenuating the uv contribution. As mentioned earlier, Fig. 12 also shows that the SiO_2 system is much less effective than the carbon-phenolic system in blocking the incident radiation flux to the surface.

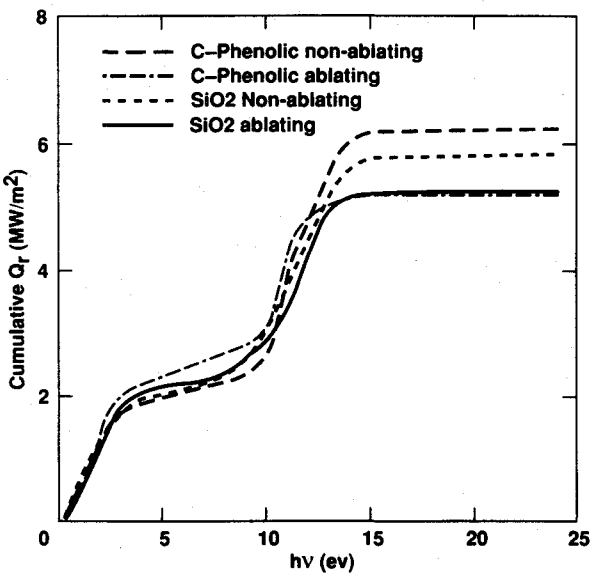

Fig. 12 Cumulative surface radiative flux comparison.

Materials Response and Surface Recession Analysis

Information obtained from the previous aerothermodynamic heating analysis can now be used to develop input for a more detailed thermal response/ablation/recession calculation for specific TPS materials of interest. The thermodynamic analysis code ACE[2] was used in conjunction with the one-dimensional charring ablator thermal response code CMA[3] to perform these materials specific calculations. Proper ablator thickness and backup insulation thickness sizing will require a complete trajectory heating pulse calculation, including the effect of any heat soak period. Required detailed trajectory information based on Fig. 2 (Ref. 1) is provided in Table 3. Included are derived quantities such as estimates of nonablating cold wall radiative heat fluxes[1] and cold wall equilibrium boundary layer heat transfer coefficients as needed input parameters for CMA. Heat transfer coeffients were based on the correlation of Marvin and Deiwert[24] for the local trajectory parameters shown in Table 3. In principle, point values of hot wall nonablating heat transfer coefficients are available from RASLE solutions at the peak heating, stagnation point. However, these values are a function of the specific material system and its associated mass and energy balance boundary conditions. Since it is important to obtain ablating CMA solutions based on the ablating RASLE results, it was decided to use the above nonablating cold wall coefficients for both carbon and silica systems and to correlate these values with RASLE through the use of a blowing correlation and the associated blowing parameter. In this manner each material system is characterized by a particular "blowing parameter." Therefore, the actual hot wall surface "convective" heat fluxes from the RASLE nonablating solutions will not agree with the cold wall, nonablative heat fluxes determined

Table 3 CMA Mars/Earth return 14 km/s trajectory input data

t, s	P_e^0, kPa	H_r, MJ/kg	Q_R^0,[a] MW/m²	$\rho_e U_e C_H^0$,[b] kg/m²-s
30	20.77	92.97	0.396	0.0342
60	27.86	86.87	5.21	0.0639
90	22.29	69.83	2.32	0.0586
120	20.36	57.29	0.821	0.0488
180	14.39	40.51	0.012	0.0439
220	12.56	32.78	0.0	0.0244
300	7.19	22.78	0.0	0.0146
340	4.86	20.16	0.0	0.0098
380	3.85	18.35	0.0	0.0049

[a]Trajectory variation estimated from Tauber et al.[1]
[b]Estimated from Marvin and Deiwert.[24]

from the Marvin and Deiwert heat transfer coefficients and trajectory recovery enthalpy.

The relative influence of mass injection obtained via the blowing parameter from RASLE is the only coupling with the CMA transient computation. The resultant agreement (or lack of agreement) between the CMA results and the steady state, peak heating ablative RASLE results will be discussed later. Using this methodology, the actual estimated values of the blowing parameter λ used in the CMA code should take on a value of $\lambda \approx 0.12$ for carbon systems and 0.55 for silica systems. In this case, λ is defined by the empirical blowing correction of the total heat transfer coefficient C_{H_0} for the shock layer, i.e.,

$$C_H(\dot{m}_s) = C_H^0 \frac{2\lambda\beta_s}{[\exp(2\lambda\beta_s) - 1]} \tag{2}$$

where $\beta_s = (\dot{m}_s/\rho_S U_S C_H^0)$, and C_H^0 is the nonblowing value of the heat transfer coefficient. Radiation heat fluxes at different trajectory points in Table 3 have been obtained by correcting Tauber et al.'s[1] cold wall, nonablating radiative fluxes obtained from published correlations for air. These have been reduced by 45% based on the calculated ablative radiative fluxes obtained from the RASLE code. This fixed adjustment is, of course, not rigorous, since it should actually be a function of flight condition along the trajectory and a function of streamwise body station. There is also a peak difference of 4% between the SiO_2 and carbon-phenolic ablative radiation blockage correction factors. A more consistent approach would be to use a radiation blowing parameter correlation similar to Eq. (2) in the CMA calculations. The computational effort to develop this correlation was not expended since the results obtained here are for TPS comparison only. Relative errors made in the radiation flux corrections are expected to be small.

CMA thermal response ablation calculations were performed for four separate TPS systems. These are carbon phenolic, carbon-carbon, Avcoat, and NASA RSI silica tile material (LI-2200). Thermal decomposition data and thermophysical properties of carbon-phenolic material were obtained from Ref. 3. Likewise, properties for carbon-carbon (nondecomposing) were obtained from the same source. Bartlett and Andersen[25] have carefully investigated the pyrolytic and charring ablative behavior of Avcoat. Silica RSI tile properties are available from Ref. 26. Additionally, a compendium of ablator properties for these materials as well as others is available from Ref. 27. Virgin material composition data are hard to obtain and are often considered proprietary. For the present modeling purposes, only thermophysical data and pyrolysis

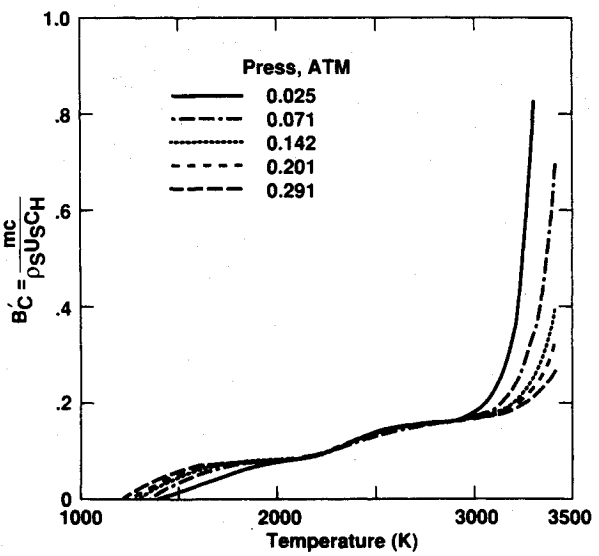

Fig. 13 B'_c curve for carbon-carbon.

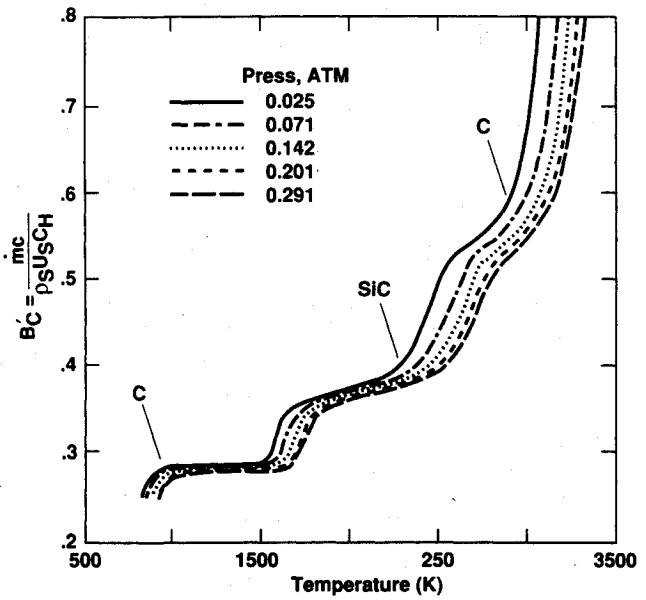

Fig. 14 B'_c curve for Avcoat.

kinetics are necessary and are available from the references. However, pyrolysis gas and residual char compositional data are necessary and are available from the aforementioned references for carbon phenolic and Avcoat. This was used for the ACE/CMA modeling. Carbon-phenolic was modeled as pure carbon char and a product pyrolysis gas composed of 53.1% C, 12.8% H, and 34.1% O by weight. Avcoat was modeled as having a residual char of composition 48.8% C, 39.7% SiO_2, 3.8% Al_2O_3, 5.1%CaO, and 2.6% B_2O_3 with an associated pyrolysis gas composed of 54.7% C, 9.3% H, 34.1% O, and 1.9% N by weight. Required for each material calculation are tables of dimensionless mass loss B'_c as a function of surface temperature and over a range of pressures encountered during the aeropass trajectory. These were obtained by standard methods using the ACE program. Additional B'_c curves for carbon-carbon and Avcoat are shown in Figs. 13 and 14. Trajectory ablation-recession calculations performed for the SiO_2 system assume that the only mass loss mechanism at these high heat fluxes is due to vaporization. In actuality, some additional mass loss will occur from melt runoff. Because of the low density of RSI and at the relative low stagnation pressures considered here, melt runoff is expected to be small (cf. Ref. 23).

Using the trajectory data of Table 3 and the previously described property data, the CMA analysis results have been obtained for each of the four TPS systems in question, and the results are presented here in Figs. 15 and 16. The carbonaceous systems undergo less recession (Fig. 16) than the RSI tile material and therefore experience higher net surface heat fluxes and temperatures. Carbon-carbon and carbon-char (carbon-phenolic and Avcoat) surfaces operate in the 3200–3400 K range, whereas SiO_2 temperatures are in the 2700–3100 K range (Fig. 15). Because the CMA calculation is a time-dependent trajectory analysis, derived material surface temperatures and ablation mass fluxes will, as mentioned earlier, deviate somewhat from those obtained from the steady-state results of RASLE. However, the results appear to be (with one exception) comparatively consistent. Carbon-phenolic results show a difference of 9% in surface temperature and 10% in ablation rate at the peak heating point (60 s) along the trajectory. For Avcoat these differences are 3 and 17%, respectively. In these cases the agreement is reasonable since the in-depth conductive heat flux is less than 25% of the net incident value. Therefore the steady-state approximation is reasonably good. Also, some of these differences are related to the fact that RASLE represents the decomposition of the ablator by assigning an overall energy of formation for the

Table 4 Manned Mars/Earth return thermal protection ablator materials comparison,[a] raked-cone geometry, $R_N = 1$ m, $V_e = 14$ km/s, $L/D = 0.5$, $\beta = 300$ kg/m^2

	Carbon[b] phenolic	Carbon-[c] carbon	Avcoat[d]	RSI (LI-2200)[e]	Avcoat (Apollo)[f]
Ablator thickness, in.	1.1	1.75	1.5	1.75	0.5–2.5
Insulation thickness, in.[g]	2.0	2.0	1.0	1.0	—[h]
Average mass loading, lbm/ft^2	9.66	17.25	5.0	3.96	1.5–7.0
TPS mass	3478	6210	1800	1425	1635
TPS weight, %	23.2	41.4	12.0	9.5	13.2

[a]Forebody heat shield only; based on nonoptimized design, i.e., uniform thickness; does not include TPS support structure.
[b]Initial density, $\rho_0 = 89$ lb/ft^3.
[c]Initial density, $\rho_0 = 108$ lbm/ft^3.
[d]Initial density, $\rho_0 = 34$ lbm/ft^3.
[e]Initial density, $\rho_0 = 22$ lbm/ft^3.
[f]Apollo entry velocity, $V_e = 11$ km/s, $R_N = 10$ ft, $\beta = 350$ kg/m^2.
[g]LI-900 RSI insulation.
[h]Apollo insulation is Q-felt/stainless steel honeycomb (Q-felt included in TPS mass).

entire composite material. CMA actually calculates an estimated pyrolysis gas production rate as separate from the char gasification process. This will alter the vapor pressure behavior (B'_c curves) for the material. CMA accounts for this and RASLE does not. The SiO_2 trajectory-recession analysis is based on a melting ablator model[23] (not CMA) and appears in excellent agreement with the steady-state model of RASLE. Surface temperatures are the same since the system operates very near the equilibrium vaporization point (Fig. 4), and ablation rates differ by less than 7%. The very low thermal conductivity of RSI tile material is responsible for the low in-depth conduction. In the case of CMA calculations for carbon-carbon, results are unsatisfactory. The conductive heat flux to the interior is actually greater than the net convective input flux. This completely invalidates any steady-state ablation assumption. Therefore the carbon-carbon results are to be considered as strictly qualitative in nature.

Finally, Fig. 16 provides a comparison of the cumulative recession obtained from CMA for each TPS material. From this vantage point carbon-carbon and carbon-phenolic materials perform the best, with very little recession. Avcoat recession is moderate (2.3 cm), and RSI (LI-2200) undergoes more significant recession (~ 4.1–4.4 cm).

An additional feature of these calculations is the use of an adiabatic backwall boundary condition for the in-depth conduction solution. In each case, several trial runs were made to choose the proper thickness of ablator material and backup insulation (in this case, assumed to be NASA LI-900 RSI tile material) to insure that the backface temperature did not exceed 450 K while keeping the ablator/LI-900 insulation interface below 1350 K (a conservative failure limit) during any portion of the trajectory, including the extended heat soak. Due to the rather wide differences in material density and thermal conductivity, large differences in these thickness values occurred (cf. Table 4). As such, these differences result in significantly different vehicle heat shield total weights. These effects are discussed in the next section.

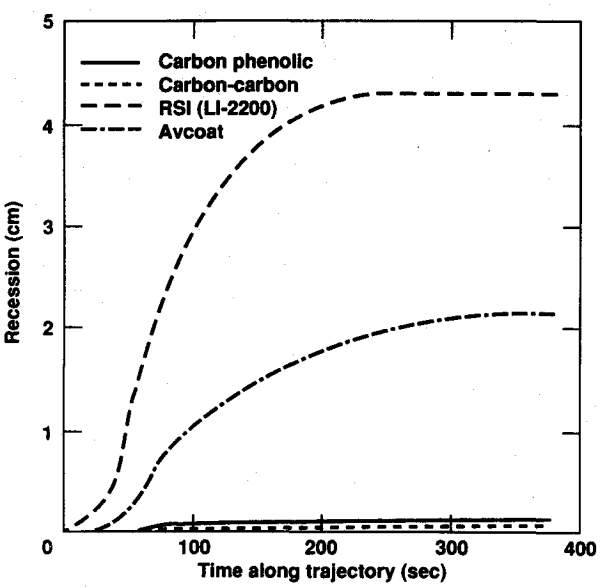

Fig. 16 Surface recession for different materials.

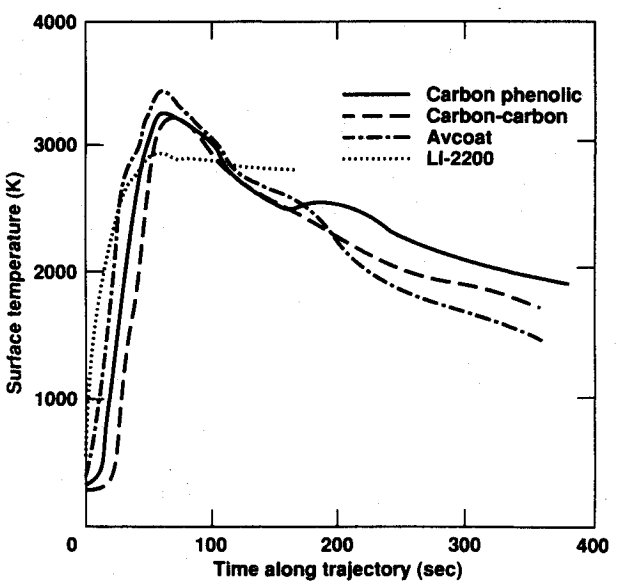

Fig. 15 Surface operating temperatures for different materials.

Heat Shield Preliminary Sizing and TPS Material Comparisons

One of the most important factors in manned Mars mission design optimization is the leverage gained in reducing the vehicle mass fraction devoted to TPS. A first order approximation of this quantity can be obtained from the previous ablation calculations for the forebody heat shield of the generic Earth return capsule shown in Fig. 1. Based on the ablator and backup insulation thicknesses determined in the previous section, the ballistic coefficient β, and the vehicle heat shield surface area, the forebody heat shield mass can be

calculated for each material system. The results of this exercise are shown in Table 4.

There are several important points to be made from the results in Table 4. The two carbon-based systems having the lowest recession rates pay the greatest weight penalty. Avcoat and RSI (LI-2200) have similar weight fractions, but Avcoat has a much more reasonable recession for the aeropass. Evidently, the final choice for an optimum ablative TPS material cannot be made by focusing on a single parameter, e.g., TPS mass fraction. If it is very important to minimize vehicle geometry change due to ablation, then the weight penalty for the carbon system (due to the additional thickness of ablator and insulation required to offset the carbon material higher thermal conductivity) may have to be paid. Depending on the mission requirements and overall vehicle size, the carbon system weight penalty can be reduced by designing it as a standoff or ejectable heat shield. Both of these options are intended to reduce insulation requirements. It is therefore necessary to be specific about the mission and arrive at a more detailed, optimized vehicle design in order to be more specific about the TPS material requirements.

Conclusions and Recommendations

It has been shown that equilibrium radiative VSL aeroheating calculations can be made for the stagnation region of entry vehicles for trajectories typical of the Mars/Earth return mission. These simulations can be done for carbonaceous and silica TPS materials ablating into air. Other systems can be modeled provided the necessary radiation model properties and parameters can be estimated or obtained from the literature. The results of the aeroheating analysis can be used to determine blowing parameters and surface incident radiation heat fluxes as input for more detailed material thermal-ablation response calculations. Except for carbon-carbon, the uncoupled material response calculations appear to agree reasonably well with the steady-state RASLE calculations. For carbon-carbon, it is necessary to perform a coupled flowfield thermal response analysis for quantitatively accurate results.

It is concluded from a material thermal-ablative response analysis that, among the four TPS materials studied, the choice of specific material for application to a generic vehicle shape is nontrivial and dependent on many other variables. More specific forebody TPS design and material specification will have to wait until the manned Mars mission studies are in a more mature state. This will enable more definitive vehicle design optimization and, therefore, provide a specific design limit for heat shield parameters. A general conclusion, of course, is that, at least near the forebody heat shield stagnation point, ablative materials will be required.

References

[1]Tauber, M. E., Palmer, G. E., and Yang, L., "Earth Atmospheric Entry Studies for Manned Mars Missions," AIAA Paper 90-1699, June 1990.

[2]Anon., "Aerotherm Chemical Equilibrium Computer Program, (ACE81)," Acurex Corp. Rept. UM-81-11/ATD, Mountain View, CA, Aug. 1981.

[3]Anon., "Aerotherm Charring Material Thermal Response and Ablation Program, (CMA87S)," Acurex Corp. Rept. UM-87-13/ATD, Mountain View, CA, Nov. 30, 1987.

[4]Braun, R. D., and Blersch, D. J., "Propulsive Options for a Manned Mars Transportation System," AIAA Paper 89-2950, July 1989.

[5]Moss, J. N., Andersen, E. C., and Bolz, C.W., Jr., "Aerothermal Environment for Jupiter Entry Probes," *Thermophysics of Spacecraft and Outer Planet Entry Probes,* edited by A. M. Smith, Vol. 56, Progress in Astronautics and Aeronautics, AIAA, New York, 1976, pp. 333–354.

[6]Nicolet, W. E., and Balakrishnan, A., "Radiating Shock Layer Environment, RASLE (User's Manual)," Acurex Corp. Rept. UM-79-10/AS, Mountain View, CA, July 1979.

[7]Gupta, R. N., Sutton, K., Moss, J. N., and Lee, K. P., "Viscous-Shock-Layer Solutions with Coupled Radiation and Ablation Injection for Earth Entry," AIAA Paper 90-1697, June 1990.

[8]Mitcheltree, R. A., and Gnoffo, P. A., "Thermochemical Nonequilibrium Issues for Earth Reentry of Mars Mission Vehicles," AIAA Paper 90-1698, June 1990.

[9]Lees, L., "Laminar Heat Transfer over Blunt-Nosed Bodies at Hypersonic Flight Speeds," *Jet Propulsion,* Vol. 26, No. 4, 1956, pp. 259–269, 274.

[10]Falanga, R. A., and Olstad, W. B., "An Approximate Inviscid Radiation Flowfield Analysis for Sphere Cone Venusian Entry Vehicles," AIAA Paper 74-758, July 1974.

[11]Nicolet, W. E., "Advanced Methods for Calculating Radiation Transport in Ablation-Product Contaminated Boundary Layers," NASA CR-1656, Sept. 1970.

[12]Wilson, K. H., and Nicolet, W. E., "Spectral Absorption Coefficients of Carbon, Nitrogen and Oxygen Atoms," *Journal of Quantitative Spectroscopy and Radiative Transfer,* Vol. 7, No. 6, 1967, pp. 891–941.

[13]Biberman, L. M., and Norman, G. E., "Recombination Radiation and Bremsstrahlung of a Plasma," *Journal of Quantitative Spectroscopy and Radiative Transfer,* Vol. 3, No. 3, 1963, p. 221 (in Russian).

[14]Peach, G., "Continuous Absorption Coefficients for Non-hydrogenic Atoms," *Memoirs of the Royal Astronomical Society,* Vol. 73, Pt. I, 1970.

[15]Henline, W. D., "Documentation of the Detailed Radiation Property Data for the Radiation-Ablation Code RASLE," NASA TM-103848, June 1991.

[16]Evans, J. S., and Schexnayder, C. J., Jr., "An Investigation of the Effect of High Temperature on the Schumann-Runge Ultraviolet Absorption Continuum of Oxygen," NASA TR R-92, 1961.

[17]Chandrasekhar, S., and Elbert, D. D., "On the Continuum Absorption Coefficient of the Negative Hydrogen Ion, V.," *Astrophysical Journal,* Vol. 128, No. 1, 1958, p. 114.

[18]John, T. L., *Monthly Notices of the Royal Astronomical Society,* Vol. 128, No. 1, 1964, p. 93.

[19]Ohmura, H., and Ohmura, T., *Astrophysical Journal*, Vol. 131, No. 1, 1960, p. 8; see also *Physical Review*, Vol. 121, No. 2, 1961, p. 513.

[20]Moore, C. E., *Selected Tables of Atomic Spectra, Atomic Energy Levels and Multiplet Tables,* National Bureau of Standards Selected Data Compilations, NSRDS-NBS 3, Gaithersburg, MD, 1970.

[21]Stull, D. R., and Prophet, H., *JANNAF Thermochemical Tables,* 2nd ed., National Bureau of Standards, NSRDS-NBS37, Gaithersburg, MD, June 1971.

[22]Yos, J. M., "Transport Properties of Nitrogen, Hydrogen, Oxygen and Air to 30,000 °K," AVCO Corp., AVCO-RAD-TM-63-7, Everett, MA, 1963.

[23]Henline, W. D., Tran, H. K., and Hamm, M. K., "Phenomenological and Experimental Study of the Thermal Response of Low Density Silica Ablators to High Enthalpy Plasma Flows," AIAA Paper 91-1324, June 1991.

[24]Marvin, J. D., and Deiwert, G. S.,"Convective Heat Transfer in Planetary Gases," NASA TR R-224, July 1965.

[25]Bartlett, E. P., and Andersen, L. W., "An Evaluation of Ablation Mechanisms for the Apollo Heat Shield Material," Acurex Corp., Aerotherm Rept. 68-38, Pt. II, Mountain View, CA, Oct. 1968.

[26]Leiser, D. B., Stewart, D. A., and Smith, M., "Rigidized Ceramic Heat Shield Materials for Advanced Space Vehicles," NASA CP 2315, Dec. 1983.

[27]Williams, S. D., and Browning, R. E., "Pathfinder Thermophysical Property Data—Thermal Protection Materials for Aerobraking Vehicles, Vol. I," Lockheed Engineering and Sciences Co., NASA Rept. (Contract NAS 9-17900) (LESC-27438), Houston, TX, Aug. 1989.

Ernest V. Zoby
Associate Editor